The Process Window for Reference Free Part Encapsulation

Elmer Lee
Paula Valdivia
Winston Fan
Sanjay E. Sarma[1]

Department of Mechanical Engineering,
Massachusetts Institute of Technology,
Cambridge, MA 02139

Reference Free Part Encapsulation (RFPE) is an automatic, universal workholding process developed by the authors and by researchers at Berkeley. In RFPE, a block of filler material encapsulates the workpiece and provides a fixturing surface, and after each machining operation, the filler block is re-filled with material to restore it to a perfect block. The objective of this research is to compute the process parameter window for RFPE. We examine the effect of process parameters such as the injection temperature, the preheating temperature, the cooling rate and the pressure on the effectiveness of the process. We show that when the temperatures are too low, or if the mold is cooled too much or too rapidly, the newly added material does not weld properly to the original encapsulation. If the temperatures are too great, then the entire encapsulation is likely to melt and lose location. The injection pressure, meanwhile, affects the surface finish of the process, and therefore the accuracy. We develop models to understand the effects of these parameters on process performance and design experiments to verify these predictions. Using these techniques, we determine the acceptable parameter windows for the process.
[DOI: 10.1115/1.1414126]

1 Introduction

In 1995, Sarma (one of the authors of this paper) and Wright developed a process called Reference Free Part Encapsulation (RFPE) at the University of California at Berkeley [1,2].[2] RFPE is a multi-setup automatic fixturing technology that uses a low melting point material to encapsulate the stock during machining. The use of low-melting point alloys is not at all new.[3] In fact, the aerospace industry has used the proces for several decades to manufacture turbine blades [3]. However, the technique as it is applied today is somewhat limiting because it is used for a single setup, to cast the fixture around the part as shown in Fig. 1. Between setups, the casting must be melted and all location information is lost. It is here that RFPE makes its contribution; RFPE makes it possible to automatically fixture in multiple setups using encapsulation fixturing, and moreover, RFPE is designed to be an automatable process. In this paper we examine the physics of the process and develop a basis for selecting the process parameters. We begin with a more detailed introduction to the process below.

1.1 Review of RFPE. Consider the imaginary scenario in which a stock of metal could be suspended midair using non-contact body forces such as, say, magnetic forces. All faces of the stock would then be exposed for machining. Any component could be machined entirely in a single ''setup'' by an appropriate machine that can access all the sides of the component. Unfortunately, it is impossible to suspend an object rigidly in this manner. Instead, we must rely on physical forces of contact to immobilize objects. Mechanisms that deliver forces by physical contact also prevent machine access in the regions where the contact occurs. For example, a vise prevents access to the clamped faces and usually to the bottom faces during milling. Thus we have the concept of setups—the object must be refixtured in a different configuration to provide access to previously hidden faces. The action of changing setups, unfortunately, entails loss of locational information. For example, when an object is released from a vise, all locational references are lost. Upon immobilization in a new configuration, these references must be re-established using further locational cues. This is a complex and time consuming task that has traditionally required human expertise and effort.

RFPE is a way to conceptually ''freeze the component in space.'' Instead of space, the workpiece is embedded in a solid block of low melting point filler material. During change of setups, the solid block of filler material is relied upon to preserve locational information. The steps taken to make a 3-D object using RFPE are described below, and shown in Fig. 2. *The stock is initially embedded within an accurate cube of the filler material.* Cubes are easy to fixture and handle automatically. The component is then machined through the filler block (which we will also refer to as the encapsulation.) At the end of the setup, the filler block is refilled and restored to a perfect block. The setup is changed, the new location and orientation of the block is known with respect to the external surfaces, and machining in the new orientation is begun.

RFPE offers potential advantages over conventional fixturing techniques. First, the range of shapes that can be manufactured using RFPE is significantly greater than by conventional machining. Parts with awkward profiles or delicate sections can be fixtured with the same effort as simpler parts. Second, process planning is simplified when RFPE replaces conventional fixturing techniques. Finally, unlike conventional fixturing devices, which have evolved over the years for human use, RFPE lends itself to automation.

1.2 The Process Window. In order for RFPE to succeed, several performance requirements must be met. First, the process requires that the surface finish of the encapsulation be high. Second, the encapsulation must be strong, especially after re-encapsulation. Finally, we must make sure that the encapsulation is accurate, and that the part remain immobile during machining.

In any manufacturing process, there are ''control variables'' which can be manipulated to maximize performance metrics. In injection molding for example, the control variables are such pa-

[1]Corresponding author. Address: Professor Sanjay Sarma, 35-010, MIT, Cambridge MA 02139, (617) 253-1925, sesarma@mit.edu.

[2]Some experimental results presented in this paper were also presented at NAMRC XXIX [2].

[3]Several materials have been used for this purpose. Issues range from mechanics, thermal properties, cutting performance, safety consideration and cost. A detailed description of which is deferred to later publications.

Contributed by the Manufacturing Engineering Division for publication in the JOURNAL OF MANUFACTURING SCIENCE AND ENGINEERING. Manuscript received Oct. 2000; revised Feb. 2001. Associate Editor: S. E. Sarma.

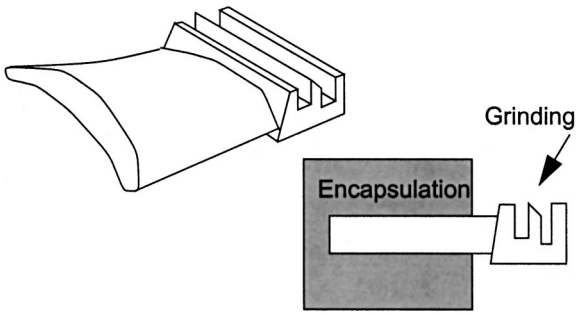

Fig. 1 Pratt & Whitney blades [Sprenkle 97]

rameters as ram pressure, chamber temperature and packing time. Careful selection of these parameters ensures that the molded parts meet quality requirements. The acceptable and feasible ranges of these process variables are referred to as the process window. In a new process like RFPE, it is necessary to first identify the process window for feasible operation. In time, rules can be developed for process optimization. This paper concentrates on determining the process window using a combination of analytical, numerical and experimental techniques. The five process parameters we examine are:

- The injection temperature
- The preheat temperature
- The cooling schedule
- The injection pressure
- The surface finish of the mold

The injection temperature and the preheat temperature are obviously related to each other and to cooling rate. We therefore examine them together in Section 2. In Section 3 we describe how pressure and surface finish interact. We conclude in Section 4. All the analysis presented in this paper pertains to a 58/42 Bismuth/Tin (Bi/Sn) alloy as the filler material, which is eutectic. The techniques developed here can be applied to other materials.

2 The Temperature Window

There are two parameters that can be controlled effectively in the molding process: injection temperature and the temperature to which the mold is preheated. A third parameter, the cooling rate, can also be controlled, though with less sensitivity. These parameters can have a significant effect on the quality of the molding process. The incremental molding process in RFPE is a somewhat delicate process; overheating can be as dangerous as underheating. We describe the problems below.

2.1 Problems Resulting From Incorrect Thermal Settings. *Poor Re-welding*. RFPE involves incremental welding. After each fill, filler material is machined away and new filler material is injected in. A weld must form between the newly injected filler and the pre-existing solid mass. If the surface of the pre-existing metal were very clean, then the bond between the new and the old material would be very good—with a yield strength in the same range as that of the original cast material. However, in reality, contaminants and oxides result in a poorer bond than desired. This can be a critical problem in machining and has exhibited itself in cracked molds as shown in Fig. 3(*a*). We refer to it as the re-welding problem. It manifests itself in brittle fracture during machining, with the crack either initiating or spreading along the re-weld interface.

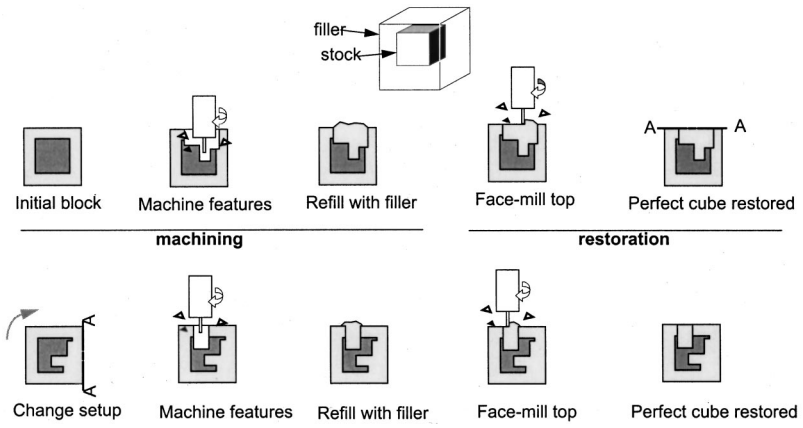

Fig. 2 Reference Free Part Encapsulation: a new prototyping technology

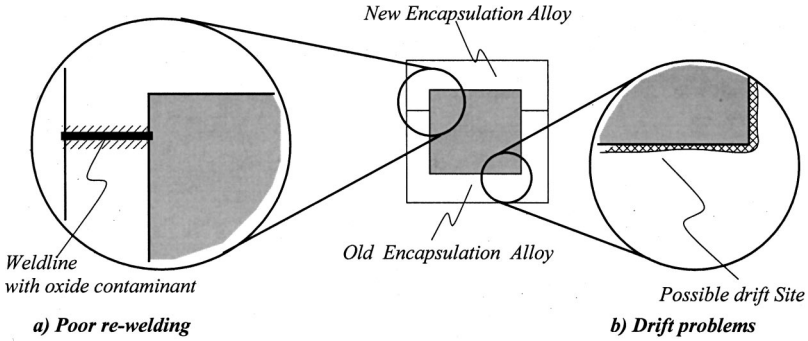

Fig. 3 Re-welding and drift problems

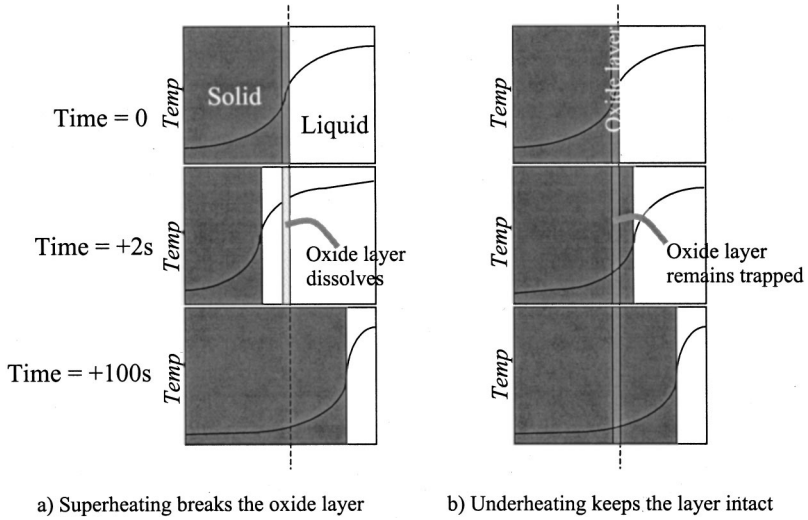

Fig. 4 Breaking down the weld by super-heating the injected metal

Drift. Temperatures that are too high can be equally destructive. Simply put, too high a temperature can result in the over-melting of the supporting filler metal, and result in the embedded block settling under gravity. This can have a serious effect on the accuracy of the process. Drift is shown in Fig. 3(*b*). Re-welding and drift were first mentioned speculatively in [1].

2.2 Addressing the Re-Welding Problem. It is well known that welds are weakened by the oxide and contaminant layers between the new and old metal. These layers impede diffusion and bonding of the two masses of material. In some cases, oxides and contaminant can be removed by dissolving them in reagents. Unfortunately, in RFPE, the use of fluxes, acids and solvents is precluded by the difficulty of automation as well as by environmental concerns.

2.2.1 The Superheating Approach. We propose that contaminants can be removed by simply *superheating* the injected metal. The superheated metal will then cause some sub-surface melting underneath the contaminant layer, dislodging and dissolving it in a larger mass of metal. With most oxide layers having a thickness ranging from 0.1 μm to 1 μm, our target melt thickness should be 2 orders of magnitude thicker, about 0.1 mm. The objective therefore is to have the solidification front move backwards about 0.1 mm or more into the solid phase before progressing forwards as shown in Fig. 4(*b*). The greater the superheating the less likely that the oxide layer will have an effect. The question that needs to be asked now is what the temperature of the liquid metal and what the pre-heated temperature of the solid metal needs to be. In addition, because the higher the temperatures, the longer the cooling time, and it needs to be understood how much active cooling is necessary and can be tolerated.

It can be shown analytically that the minimum temperature required of the liquid, T_l, for the solidification front to retreat *infinitesimally backward* as shown in Fig. 4(*a*) is:

$$T_l = \frac{((k_s\rho_s C_{ps})^{1/2} + (k_l\rho_l C_{pl})^{1/2})T_m - (k_s\rho_s C_{ps})^{1/2}T_s}{(k_l\rho_l C_{pl})^{1/2}}, \quad (1)$$

where k, ρ and C_p are the coefficient of thermal conductivity, density and specific heat respectively, with subscripts s and l indicating solid or liquid, and where T_m is the melting point of the filler material, and finally, where T_s is the temperature of the solid phase. Equation (1) is derived simply from an analysis of two semi-infinite bodies instantaneously in contact [4].

Equation (1) only applies if we are looking at the instantaneous retreat of the front. However, the question we would ideally like to answer is under what conditions the front will retreat a set amount, say 0.1 mm. Unfortunately, because of the phase change involved, it is difficult to derive a similar analytical equation relating solid and liquid phase temperatures such that there is a given penetration depth. Instead, for this more complicated situation, numerical analysis is necessary. We describe it below.

2.2.2 Simulation of Phase Change. We developed a simulation package which uses the Runge-Kutta method of Order 4 to solve the differential equation for heat transfer. After the materials to be simulated are designated, the solver breaks down each layer into nodes of a specified displacement step size. The simulation was written in Labview™. The dataflow representation of Labview results in surprisingly efficient computation for the copious amounts of data we needed to generate in our analysis. The equations of heat transfer, of heat conduction through a solid and of

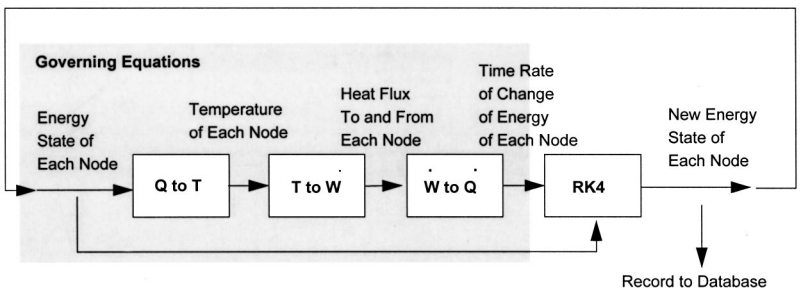

Fig. 5 Diagram of the algorithm to solve the heat transfer problem using Runga Kutta and the proper governing equations

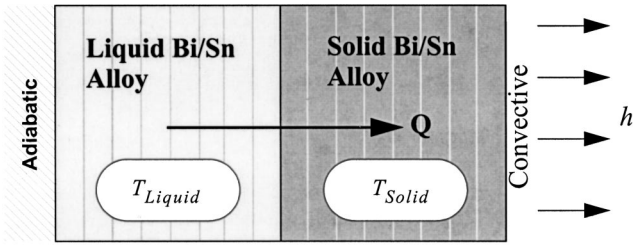

Fig. 6 Modeling heat transfer for re-welding

energy exchange during phase change are applied to each node. In order to track the phase change correctly, the internal energy of each node is tracked instead of its temperature. This is shown in Fig. 5. Knowing the energy states allows one to determine not only the temperature of the node but also the phase. On the hot end of the model, an adiabatic condition is assumed. On the other end, an ambient temperature and heat transfer coefficient can be prescribed and applied. This is shown in Fig. 6.

To optimize processing time, the time step can be programmatically varied. As shown in Fig. 6, the re-welding simulation consists of a 2 layer model of the Bi/Sn eutectic. The first layer is in solid phase and the second in liquid. Each layer is 0.0127 meters thick (0.50 in.) and is held at a specified initial temperature. At time 0, the two layers are brought into instantaneous contact and the heat transfer is simulated. While one end-condition is an adiabatic surface the other surface is subjected to convective cooling at a specified heat transfer coefficient.

We define a nondimensional initial condition Θ given by:

$$\Theta = \frac{(T_l - T_m)}{(T_m - T_s)}. \tag{2}$$

As expected, the simulation shows that rewelding initiates when Θ is approximately 1. Note that this condition follows from Eq. (1) when k, ρ and C_p are the same for the solid and the liquid phases. The results of the simulation are summarized in Fig. 7. At $\Theta = 1$, neither side will change phase and below unity, the liquid with start to solidify first. The simulation can also illustrate a more complex behavior than the simple analytical semi-infinite body model. The semi-infinite model is only appropriate for either very large bodies or for very short periods of time, and it cannot demonstrate a melt front retreating into the solid region before moving forward. The simulation on the other hand is able to show the retreating solidification front. The maximum depth for which the melt front travels into the solid is here designated as the maximum penetration depth and it is the variable we are seeking to study.

From Figure 7, we can recognize that not only is the quantity Θ important in determining the maximum melt depth, but that the individual injection and preheat temperatures do play a role in the maximum penetration depth of the melt front. One sees that with higher injection temperatures, a greater melt depth is achieved for a given Θ. It could be surmised that the highest possible temperature for injection will provide the most benefit for the encapsulation process. However, the injection temperature must be limited by other practical considerations. For example, it has been observed that an increase in injection temperature will increase the oxidation rate of the liquid encapsulation alloy. With a greater amount of oxidation, the encapsulation alloy will not perform as well during the encapsulation process. In later sections, we will also discuss the problems of drift.

From the graph in Fig. 7, it can also be seen that melting in general begins when Θ is slightly above unity. In the third case, where the convective heat transfer coefficient is higher, we see that a perceptible amount of melting does not occur until Θ is close to 1.5. One can conclude that for the simulated geometry, the convective end condition *will* affect rewelding, and it is thus recommend that cooling is not begun immediately so as not to hinder welding. Figure 8 shows the solidification front simulated against time for a range of conditions. It can be seen that the solidification front first retreats before marching forward, as described. Furthermore, we can see that the front reaches its maximum penetration before 20s. Therefore, we can also use this data to determine when to start cooling the mold. In general, we have run hundreds of simulations like the ones shown, and we are able to conclude that rapid active cooling can and should be begun about 20s after the injection has been completed.

From the information generated by the simulation, one can conclude that for an injection temperature of about 180°C, the solid encapsulation needs to be preheated to about 110°C to achieve the desired 0.10 mm of melt penetration depth. While increasing the preheat temperature will surely increase the penetration depth, we must examine how the preheat temperature will affect our second issue, that of over-melting and drift. We will do so in Section 2.3

2.2.3 Experiments. We conducted a series of experiments to validate the results shown [5]. Our experimental setup consisted of a mold shaped like an ASTM tensile test specimen, which we half filled with molten Bs/Sn and cooled, then preheated to a temperature T_s. We then injected in molten Bs/Sn heated to a temperature T_l and waited for it to freeze, simulating a re-weld. We conducted tension tests on a series of such specimens at dif-

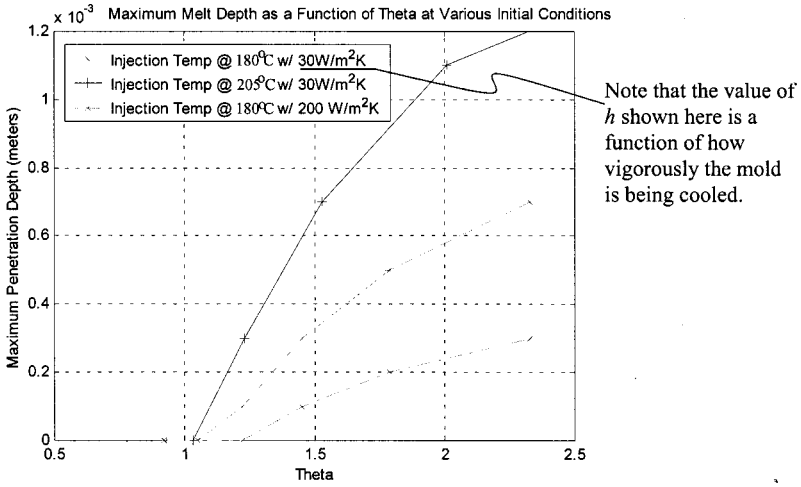

Fig. 7 How the maximum penetration depth changes with Θ for given cooling rates

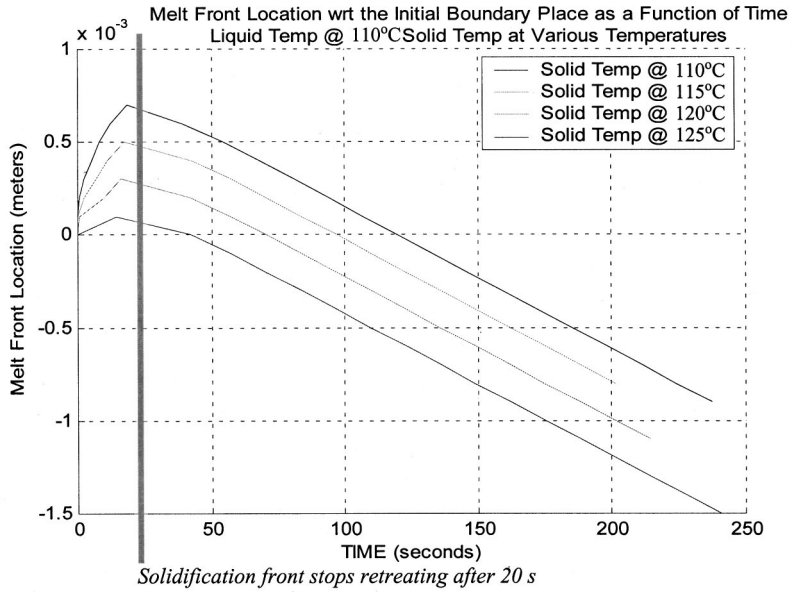

Fig. 8 The temporary retreat of the solidification front as predicted by the simulation

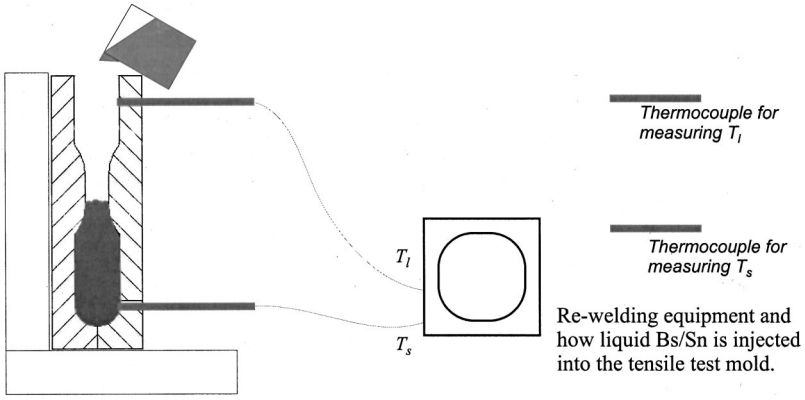

Fig. 9 The re-welding mold and process

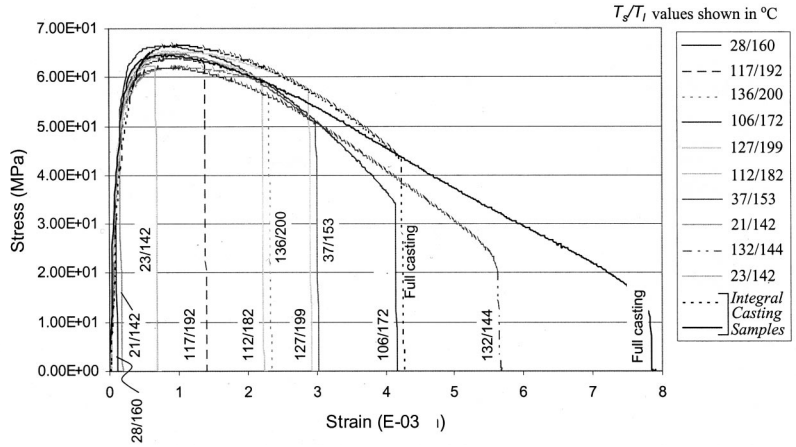

Fig. 10 Tensile test results for re-welds in different regimes

ferent T_s & T_l combinations to understand how the parameters T_s and T_l affected tensile behavior. The mold and process are shown in Fig. 9. Because of the expense involved in controlling T_s and T_l exactly, we chose in our experiments to do a number of experiments with a range of T_s & T_l values.

The results of the tension test are shown in Fig. 10. It can be seen broadly that the greater the values of T_s & T_l, the more ductile the behavior of the re-weld. This is not always the case, but appears to be a trend. We also include the results of two full castings for reference—samples manufactured without a reweld as

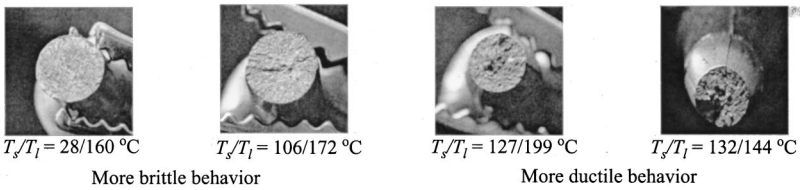

Fig. 11 Pictures of failed section showing increasing ductility

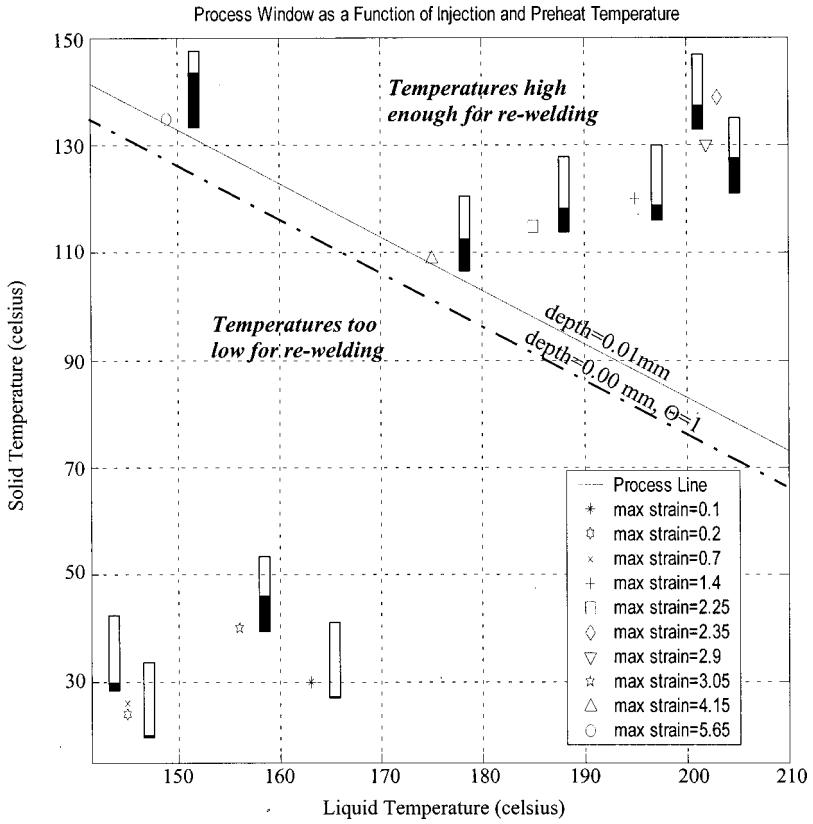

Fig. 12 The process window for re-welding with tensile test results superimposed

one integral casting. In general the ductility can also be observed in the appearance of the failed region; the higher the re-welding temperatures, the more pimpled the surface appears, as shown in Fig. 11. These results are summarized to show the trend more clearly in Fig. 11. The lines shown indicate the $\Theta = 1$ line and the line for a penetration depth of 0.1 mm. The region above the lines indicates the acceptable range of temperatures to prevent re-welding. We also indicate the temperatures of the tensile test specimens and their performance on the same graph to show the dependence of behavior on T_s and T_l.

2.3 Preventing Drift. The results of the previous section, summarized in Fig. 12, showed clearly that the higher the preheat temperature and the injection temperature, the better the weld. However, too high a temperature can also be detrimental, not only because it increases cooling time and therefore cycle time, but also because it causes drift as described earlier. In this section we examine the upper temperature limit for preventing drift. Because experimental verification of drift is difficult, we rely on numerical analysis for this estimation.

The drift simulation consists of a 4 layer 1-D heat transfer model. The first layer is liquid Bi/Sn alloy, 0.0635 meter thick. The next is a piece of 0.127 meter thick of aluminum 6061-T. It is followed by a solid layer of Bi/Sn, 0.0635 meter thick. Lastly a 0.0635 meter thick piece of stainless steel is placed at the end. Again, the end conditions are given to be adiabatic on end and convective on the other. The dimensions are representative of the

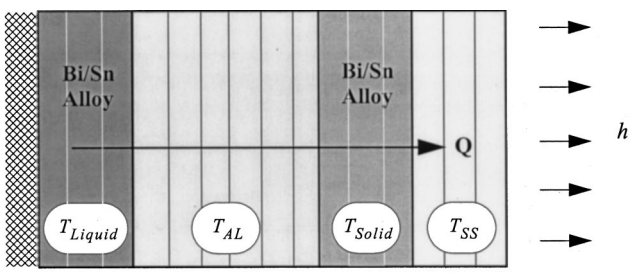

Each vertical rectangle represents an element in the numerical method.

Fig. 13 Simulation for predicting re-welding

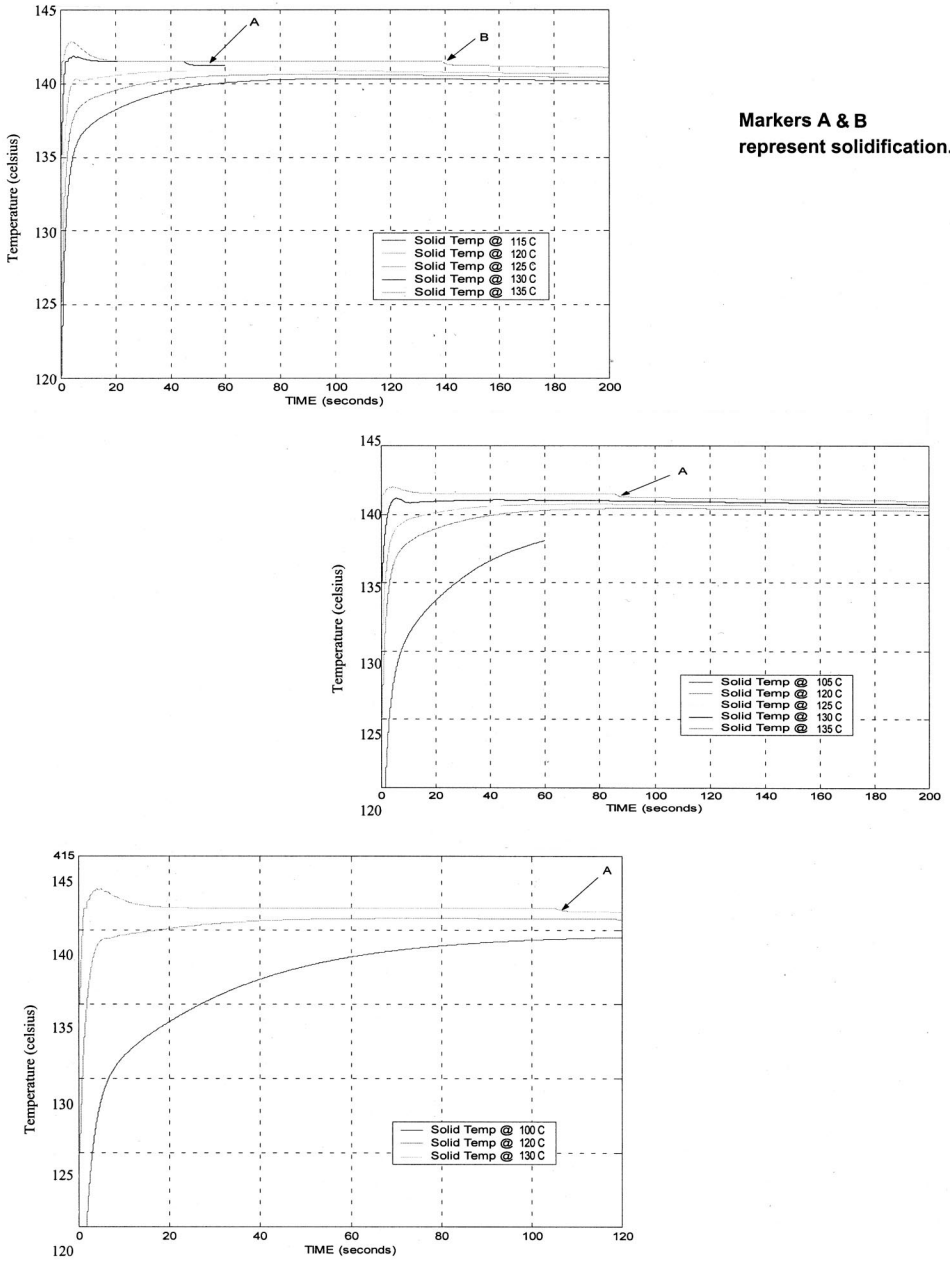

Fig. 14 Results of simulation for drift

typical RFPE molding operation, and the model represents an aluminum block encapsulated in Bs/Sn in a steel mold. This is shown in Fig. 13.

Figure 14 summarizes the output from the heat transfer simulation. The figure shows that a preheat temperature of 110°C will not initiate drift even when the injection temperature is as high as 230°C. At an injection temperature of 180°C, drift begins when the preheat temperature is between 135°C and 140°C. At 205°C, drift will begin when preheat is between 130°C and 135°C. At 230°C, drift begins between 125°C and 135°C. One observes that even with large changes in the injection temperature, the preheat temperature needed to initiate drift does not vary that greatly. One can thus conclude that *the preheat temperature is the dominant variable that controls drift*. With the melting point of the Bi/Sn eutectic being 138.5°C, one observes that drift only occurs when the preheat temperature is very near the melting point. Thus the robustness of the encapsulation process in terms of developing a good reweld strength while preventing drift can be considered very high. With an injection temperature of 180°C, the preheat temperature can vary some 25 degrees, from 110°C to 135°C, and still result in a good encapsulation.

2.4 Summary. The findings from this section are summarized below. They result in the composite temperature process window shown in Fig. 15, and also significantly affect the design of the equipment [7].

- Re-welding can be assured by a combination of a high injection temperature and a high solid preheat temperature, which result in an initial retreat of the solidification front.
- Sufficient retreat of the solidification front is usually achieved within the first 20 seconds.

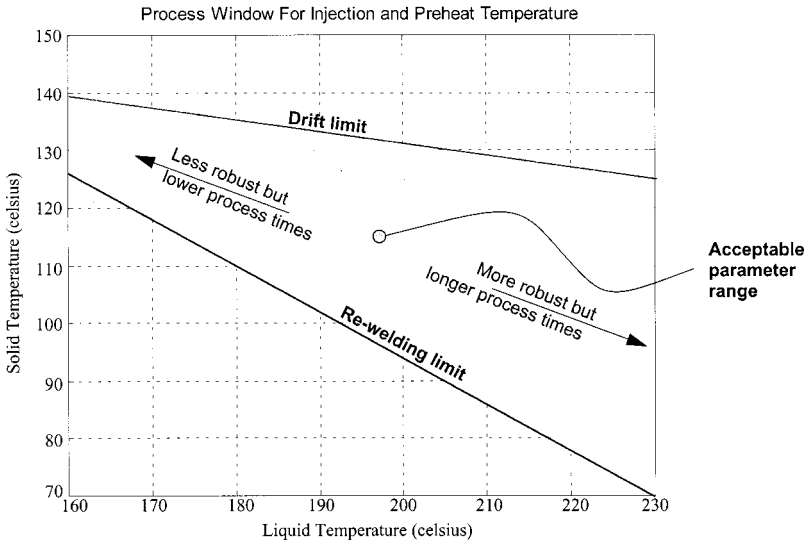

Fig. 15 The process window for pre-heat and injection temperatures

- Drift usually begins after 40 seconds. Therefore, cooling must be begun after 20 seconds but before 40s.
- Drift can be virtually eliminated by keeping the solid preheat temperature below 230°C.

3 Pressure and Surface Finish

For reasons of convenience and practicality, it is desirable that the injection pressure requirements of the RFPE process be low, in the order of 350–700 KPa (50–100 psi). Lower pressures require lower clamping forces and therefore smaller structures, and perhaps more importantly, with lower pressures it is possible to use standard shop air supplies or standard pneumatic compressors. Pressures in these ranges qualify RFPE as a type of low-pressure die-casting system. One of the questions that arises in low pressure systems is whether it is possible to achieve high enough a surface finish. This question is especially pertinent in RFPE because the surfaces are used as fixturing datums. In this section, we examine the relationship between surface finish and pressure, and determine the acceptable range of pressures.

We begin by asking what the required surface finish of the encapsulation block is. We address this question below from a contact mechanics point of view. In Section 3.2, we ask the next question: how do the injection pressure and the finish of the mold affect the finish of the encapsulation?

3.1 Required Surface Finish of the Encapsulation Block. We state that the tolerance required of RFPE is 25μm, which corresponds to 0.001 in., a standard machining target. There are two kinds of errors that can affect this tolerance: form error and surface roughness. Form error can be measured and compensated for every encapsulation block. However, surface asperities can cause surface deformation which is difficult to predict or compensate for in process. Asperities are known to reduce contact integrity because the area of contact is usually significantly less than the nominal area [8]. This is shown in Fig. 16. We analyze this problem in the current section and conclude with an order of magnitude argument: that if the roughness of the surface is better than 12 μm R_a, then the surface deflection will not significantly affect the tolerance of the process. The explanation for this conclusion follows.

Under fixturing load, the asperities deflect elastically and plastically. In the elastic case, it has been proposed in the literature that the contact between two rough surfaces can be treated as contact between a flat surface and a surface of effective roughness $\sigma=\sqrt{\sigma_1^2+\sigma_2^2}$ and effective elastic modulus E^*, given by $1/E^* = 1-\vartheta_1^2/E_1+1-\vartheta_2^2/E_2$, where σ_1 and σ_2 are the RMS roughness values, E_1 and E_2 are the elastic moduli, and ϑ_1 and ϑ_2 are the Poisson ratios of the original surfaces [9]. Assuming a simple sinusoidal surface model, it can be shown that the limit of elastic deflection, δ_y, after which the material flow becomes plastic is:

$$\delta_y=\frac{81}{16}\frac{\pi^2 Y^2 R}{E^{*2}}, \tag{3}$$

where R, E^* and Y are the radius of curvature of asperities, elastic modulus and yield strength of the material respectively [10]. By

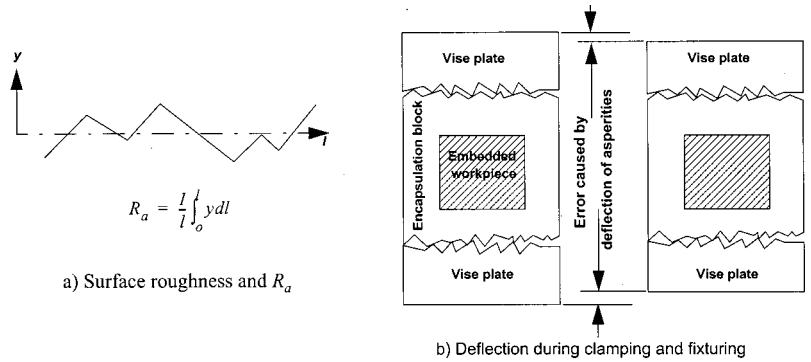

Fig. 16 Surface roughness under fixturing load

inserting the material constants of cast Bi/Sn and computing δ_y, it can be shown that for machined surface finishes, δ_y is insignificant and that the plastic deformation will dominate. There has been a significant amount of research into the plastic deflection of asperities. Beginning with Moore's work in 1948 [11], followed by others [8,12], researchers have noted that asperities persist even under extremely high compressive loads. In some cases, researchers have been able to measure pressures in compressive tests approaching six times the yield strength and the asperities still exist [13,14]. Most of these studies show that asperities eventually become, on a per area basis, stronger than the bulk material. As a result, they transmit the load to the bulk material like structural members. This behavior is complex and it is hard to predict the exact deflection of a surface in plastic flow.

We, however, make a bounding argument. Recognizing the fact that plastic flow is incompressible, we make the argument that the maximum deflection of the asperities must be, at most, R_a. In 2D, where the deviation from a center-line is given as $y(l)$, R_a is defined as $1/l\int_0^l y dl$. The definition of the center-line, meanwhile implies that $\int_0^l y dl = 0$. This proves that the material in the peaks can at most fill the valleys. Therefore, if the material behaves in this way, the plastic deflection, which is the significant portion, can at most equal R_a. In practice, the asperities resist plastic flow beyond a point. Therefore, the plastic deflection will usually be less than R_a. We therefore set the requirement that the surface roughness of the encapsulated block must not be worse than $R_a = 12\ \mu$m.

3.2 Surface Finish Replication. As one might expect, the surface finish of an encapsulation block depends on the surface finish of the die itself, and on the pressure of the injection process. We refer to this transference of finish from mold to encapsulation surface as *surface replication*. Given that we would like to imprint a finish of $R_a = 12\ \mu$m on the encapsulation, we ask what combinations of pressure and die surface finish are acceptable.

There is a small amount of literature on this topic. Experimental studies of the effect of squeeze casting pressure primarily on microstructure, and to a smaller extent on porosity and surface finish is presented in [15,16,17]. The results show that increasing pressure improves the replication and the researchers argue that higher pressures force the molten metal into the surface more effectively. However, research has tended to be restricted to aluminum at very high pressures, in the range of 50 MPa, and does not directly apply to the situation described here.

A related topic is porosity, which does affect surface finish. There is a significant amount of previous work dealing with porosity, but the results have tended to be very specific to the materials, geometries and boundary conditions involved [6]. The modern approach uses criteria functions, which are combinations of several thermal properties such as cooling rate R_c, thermal gradient G, solidus velocity V_s and solidification time t_s [18]. Unfortunately, the criteria functions themselves are material dependent, and no results are available in the literature for Bi/Sn. For example, the functions for steel and aluminum alloys respectively are $G/\sqrt{R_c}$ and $G \times t_s^{2/3}$ respectively [19,20]. Furthermore, the understanding we seek for the purposes of RFPE are fairly narrow; we simply ask how well surfaces are replicated as a function of mold finish and pressure, and a more detailed analysis seems unnecessary. Few analytical methods exist which can be generalized. Under these circumstances, experimentation remains the only recourse, and we explain it here. In order to understand the process window for good replication, we conducted a series of experiments on imprinted surface finish.

3.2.1 Equipment and Procedure. The experiments worked as follows. We replicated a range of standard surfaces of different roughnesses on Bi/Sn encapsulations injected at different pressures. We then measured the imprinted surfaces to see how the quality of the imprint was affected by pressure. The idea was to see how the surface roughness of the surface being imprinted and the injection pressure affected the replication.

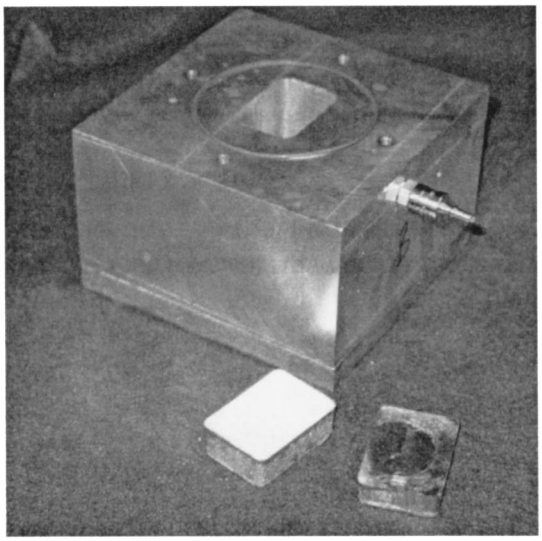

Fig. 17 Mold for Bi/Sn replication test

A low-pressure mold, shown in Fig. 17, was manufactured to produce Bi/Sn specimens with varying surface roughnesses across a range of pressures. The bottom plate of the mold was designed to hold surface roughness standards from the Gar Electroforming M-15 Surface Roughness Standard Set. A connector that attached from above was used to inject molten Bi/Sn at different pressures. A KLA-Tencor P-10 Profilometer was used to evaluate the surface of the specimens after the replication experiments.

To produce each specimen, the appropriate surface roughness insert was cleaned and placed on the bottom plate and secured to the mold body. The mold was heated to 150°C. Molten Bi/Sn alloy was then injected into the mold. The top plate was then secured and the mold pressurized to the desired pressure. The specimens were produced at atmospheric pressure and 40 psi, 60 psi, and 80 psi above atmospheric pressure. For each pressure level, surface roughness standards of 0.1 μm, 0.4 μm, 1.6 μm, and 3.2 μm were used. Because of the high cost of these experiments, only 16 separate experiments were conducted.

3.2.2 Results. The results of the experiment are shown in Fig. 18. There are essentially four sets of data, connected by solid lines. Each set presents the measured surface finishes of the imprinted surfaces as pressure changes for a given reference surface. Each dataset is accompanied by a dashed baseline, which shows the associated nominal reference value.

It is easy to see that as the pressure increases, surface finish approaches the reference value. Also, it is clear that the better the surface finish of the reference surface, the better the finish of the imprinted surface. Both these trends are as one would expect intuitively. The greyed out region on the left sides of the graph indicate that the data is unreliable because the roughness exceeded the limit of the profilometer. However, the trends in this region are still apparent.

The intersections of the lines shown in Fig. 18 with the 12μm line give us the acceptable pressures for different reference finishes. This data is represented explicitly in Fig. 19. The figure shows the acceptable surface finishes for different pressures of injection. Clearly, the higher the injection pressure, the less exacting the requirement on the surface finish of the mold. The region on the right is essentially the feasible process window.

The conclusions from this experiment can be summarized as follows. First, we have concluded in this section that a surface

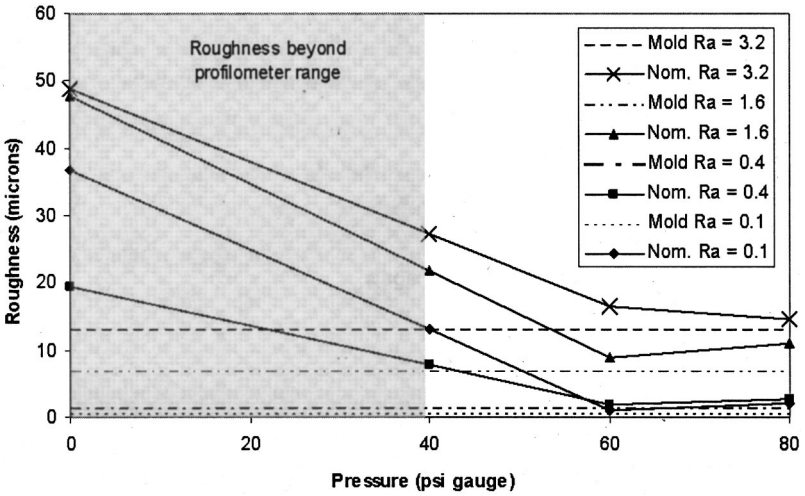

Fig. 18 Experimental results from imprint tests

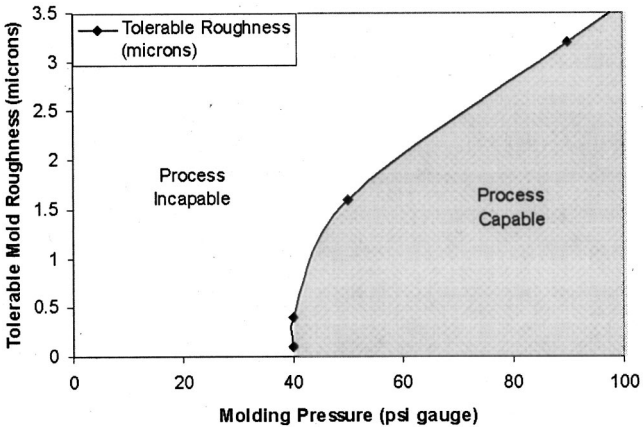

Fig. 19 Process window for pressure and surface roughness

finish of $R_a = 12\ \mu$m is sufficient for RFPE. We have shown that the pressure and the surface finish of the mold together determine the surface finish of the imprinted (molded) surface. It is further possible to deduce from Fig. 19 that:

- Molding pressure should be at least 40 psi. In other words, gravity pouring is not sufficient.
- Furthermore, if we assume that shop air is at about 60 psi, then $R_a = 2\ \mu$m is required. This means that the surface should be *ground* after milling.

These results justify low-pressure die casting. This is crucial in the design of the process. In [7] we describe the machines designed with this assumption.

4 Conclusions

We have presented a comprehensive analysis of the process parameters that control the performance of RFPE. We examined the temperature requirements from the point of view of re-welding and melting. We developed analytical and numerical models for re-welding. We also conducted extensive experiments to validate the model. We observed that the higher the injection temperature and the higher preheat temperatures in general resulted in more ductility along the interface of the re-welding. For re-melting, analytical models are difficult to develop. We instead developed a numerical analysis and computed the required limit line. The result of our analysis was a process window graph.

We then examined pressure and surface finish requirements. Through a series of experiments, we computed the range of acceptable temperatures and surface finishes for the process. As expected, the greater the pressure, the better the surface finish of the encapsulation. Similarly, the better the finish of the mold, the better the finish of the encapsulation.

The results of our analyses and experiments provide the required process windows. In particular, we noted that the acceptable range of temperatures is fairly broad, and that the process is relatively robust. We also note that there is definitely pressure requirement which can be met by low pressure die-casting. Higher pressures are not required, but at the same time, gravity casting will not suffice. This is an important finding because it enables our process to become inexpensive and portable, and it profoundly affects the design of our equipment. Finally, we concluded that the process requires a ground mold. If the finish of the mold is not ground, the imprinted surface finish will be poorer than can be tolerated.

The research reported in this paper helps us in several ways. First, it helps us establish the requirements for the design of the process equipment. For example, in addition to the conclusion on pressure above, we have also concluded that active cooling is necessary. Second, it guides the selection of the filler material. The 58/42 Bi/Sn we have used offers robust performance. Other materials may be cheaper, but need to be analyzed in the same way for performance. Third, the process windows we have computed indicate to us how the process can be optimized for performance. Performance metrics that can be optimized include cycle time and accuracy. We will present our findings in these areas in future publications.

Acknowledgments

We acknowledge the support of NSF and the support of the KIMM-MIT program. We acknowledge the assistance of Ms. Ceani Guevara and Mr. Doo-Sun Choi.

References

[1] Sarma, S., and Wright, P. K., 1996, "Reference Free Part Encapsulation: A New Universal Fixturing Technology and its Implications on Design and Planning," J. Manuf. Syst., **16**(1), pp. 35–47.
[2] Lee, E., Valdivia, Paula, Fan, Winston, and Sarma, Sanjay E., 2001, "Temperatures and Pressures for Encapsulation Fixturing," *Transactions of the North American Manufacturing Research Conference* (NAMRAC XXIX), Society of Manufacturing Engineers.
[3] Sprenkle, J. B., 1998, Personal Conversation at Pratt & Whitney, September.
[4] Mills, A. F., 1995, *Basic Heat and Mass Transfer*, Irwin Publishing, Chicago.

[5] Valdivia, P., 2000, ''Investigation of the Remolding Step in Reference Free Part Encapsulation,'' S. M. Thesis, Massachusetts Institute of Technology.
[6] Allsop, D. F., and Kennedy, D., 1983, *Pressure Diecasting; Part 2*, Pergamon Press, New York.
[7] Lee, E. C., 1999, ''Development of an Encapsulation Process for use in a Universal Automated Fixturing System,'' S. M. Thesis, Massachusetts Institute of Technology.
[8] Greenwood, J. A., and Rowe, G. W., 1965, ''Deformation of Surface Asperities during Bulk Plastic Flow,'' J. Appl. Phys., **36**, pp. 667–668.
[9] Johnson, K. L., 1985, *Contact Mechanics*, Cambridge University Press, Cambridge, U.K., pp. 397.
[10] Fan, W., 2000, ''The Effect of Surface Roughness on the Precision of the Encapsulated Fixturing System,'' S. M. Thesis, Massachusetts Institute of Technology, p. 36.
[11] Moore, A. J. W., 1948, ''Deformation of Metals in Static and in Sliding Contact'' Proc. R. Soc. London, Ser. A, **A195**, pp. 231.
[12] Williamson, J. B. P., and Hunt, R. T., 1972, ''Asperity Persistence and the Real Area of Contact Between Rough Surfaces,'' Proc. R. Soc. London, Ser. A, **A327**, pp. 147.
[13] Childs, T. H. C., 1973, ''The Persistence of Asperities in Indentation Experiments,'' Wear, **25**, pp. 16.
[14] Uppal, A. H., and Probert, S. D., 1972, ''Deformation of Single and Multiple Asperities on Metal Surfaces,'' Wear, **20**, pp. 381.
[15] Kim, S-W, Durrant, G., Lee, J-H., and Cantor, B., 1999, ''The Effect of Die Geometry on the Microstructure of Indirect Squeeze Cast and Gravity Die Cast 7050 (Al-6.2Zn-2.3Cu-2.3Mg) Wrought Al Alloy,'' J. Mater. Sci., **34**, pp. 1873–1883.
[16] Skolianos, S. M., Kiourtsidis, G., and Xantzifotious, T., 1997, ''Effect of Applied Pressure on the Microstructure and Mechanical Properties of Squeeze-Cast Aluminum AA6061 Alloy,'' Mater. Sci. Eng., A, **A231**, pp. 17–24.
[17] El Mahallawy, N. A., Taha, M. A., and Zamzam, M. L., 1993, ''On the Microstructure and Mechanical Properties of Squeeze-Cast Al-7 wt % Si Alloy,'' J. Mater. Process. Technol., **40**, pp. 73–85.
[18] Huang, H., Suri, V. K., Hill, J. L., and Berry, J. T., 1993, ''Issues in Thermal Contact and Phase Change in Porosity Prediction,'' Trans. ASME, **115**, pp. 2–7.
[19] Niyama, E., Uchida, T., Morikawa, M., and Saito, S., 1982, ''A Method of Shrinkage Prediction and its Application to Steel Casting,'' AFS Cast Metals Research Journal, **7**, pp. 52–63.
[20] Lee, Y. W., Chang, E., and Chieu, C. F., 1990, ''Modeling of Free Behavior of Solidifying Al-7Si-0.3-Mg Alloy Plate Casting,'' Metallurgical Trans., **21B**, pp. 715–722.